Theta oscillations optimize information rate in the hippocampus

Adrián F. Amil[1, †, *], Albert Albesa-González[2, †], and Paul F.M.J. Verschure[1]

[1]Donders Institute for Brain, Cognition and Behaviour - Radboud Universiteit, Nijmegen, Netherlands
[2]Imperial College London, London, United Kingdom
[†]These authors contributed equally to this work
[*]*Correspondence to* adrian.fernandezamil@donders.ru.nl

December 8, 2022

Abstract

Low-frequency oscillations shape how neurons sample their synaptic inputs, hence regulating information exchange among neural circuits. In the hippocampus, theta oscillations (4-8 Hz) enable the temporal organization of cortical inputs, resulting in a phase code. However, the advantages of the specific theta band over other frequency ranges remain unclear. It is possible that this specific frequency range is optimizing a trade-off between information throughput and biophysical constraints of the neuronal substrate. To test this hypothesis, we analyze a physiologically constrained model of the rodent hippocampus comprising stochastic leaky integrate-and-fire neurons driven by oscillations. By estimating the information rate of the phase code for a range of noise and frequency levels, we identify a trade-off between sampling frequency and coding precision. We observe that, under physiological noise levels, theta-band oscillations optimize the speed-precision trade-off, maximizing information rate. Further, we demonstrate that theta optimizes this trade-off throughout the entire dorsoventral axis of the hippocampus with its pronounced gradients of several physiological properties. In addition, we find that maintaining an optimal information rate relies on the concurrent modulation of both frequency and amplitude, hence explaining the locomotion speed-dependent modulations of the hippocampal theta oscillation that are observed in rodents and humans. Overall, our results suggest that low-frequency oscillations are adapted to maximize the information rate of neural sampling given the temporal and biophysical constraints under which neural circuits operate.

Author Summary. In the hippocampus, a prominent oscillation in the theta band (4-8 Hz) allows single neurons to rhythmically sample and represent the ever-changing input signals coming from the cortex. However, it remains unclear why this hippocampal rhythm lies within the theta band. Here, we show that neurons that use oscillations to sample noisy input signals face a trade-off between their sampling speed (i.e., the frequency) and their coding precision (i.e., the accuracy of the representation). We find that, for simulated hippocampal neurons, this trade-off is optimized precisely within the theta band. Importantly, our framework allows us to explain other fundamental properties of the hippocampus while having implications for other brain areas that might use similar sampling mechanisms. In summary, we provide an explanation as to why oscillations in the hippocampus are confined within the theta band, and lay down the foundations to study how properties of single neurons determine the optimal sampling frequencies in a particular neural circuit.

1 Introduction

Early physiological experiments with rodents showed that hippocampal place cells (i.e., neurons whose firing rate is higher in particular locations of the environment) progressively fire to earlier phases of the oscillating local field potential (LFP) as the animal traverses the place field (O'Keefe and Recce, 1993). This finding of phase precession in the hippocampus fostered further research that aimed at clarifying the precise relationship between behavior and the neuronal firing times with respect to the prominent theta-band (4-8 Hz) oscillation. Notably, it was shown that the reconstruction of the animal's position was greatly improved by considering the phase of firing along with the corresponding firing rates (Jensen and J. E. Lisman, 2000). These findings firmly established the notion of phase coding as a plausible alternative to firing rate coding in explaining how information is represented in neural circuits (J. Lisman, 2005). The phenomenon of the hippocampal phase precession also led to theories and computational models that tried to explain such a temporal progression of spikes across the theta phase. One of the most successful models so far has been the rate-to-phase transform, whereby rate-coded inputs from the entorhinal cortex drive hippocampal neurons to fire earlier or later depending on the input strength, hence transforming the entorhinal inputs into phase-coded hippocampal representations (McLelland and Paulsen, 2009; Mehta, Lee, and Wilson, 2002). This rate-to-phase transform received further empirical support from outside of the hippocampus (Margrie and Schaefer, 2003), suggesting that it could be a more general mechanism of information encoding operating in sensory-related areas (J. Lisman, 2005).

Theories trying to link the oscillatory nature of brain activity with cognitive function have been proposed (Buzsáki and Draguhn, 2004). It is indeed appealing to relate the rate-to-phase transform with the notion of synaptic sampling (Buesing et al., 2011). That is, low-frequency field oscillations modulate the neurons' excitability (either directly by ephaptic effects (Anastassiou et al., 2011) or indirectly by feedback inhibition (Fries, 2015; Mizuseki et al., 2009)), so that rate-based inputs are rearranged in time based on their respective rate levels. Therefore, by leveraging a rhythmically-organized first-spike latency code (VanRullen, Guyonneau, and Thorpe, 2005), a properly time-referenced phase code can be used to sample synaptic inputs, with independent samples being drawn at every new cycle. In turn, this rhythmic neural sampling from sensory-related areas would give rise to the perceptual sampling effects observed at the behavioral level (Caplette, Jerbi, and Gosselin, 2022; Korcsak-Gorzo et al., 2022; VanRullen, 2016). On the one hand, the notion of rhythmic neural sampling is consistent with the widely reported membrane time constants of pyramidal cells (of the order of 10 to 30 ms) being much shorter than the period of the observed low-frequency field oscillations (ranging from around 100 ms to 1 s), hence allowing a proper reset of the activity in a cycle-to-cycle manner. Then, on the other hand, experiments combining behavior and electrophysiology support the perceptual sampling hypothesis by showing that stimulus detection is modulated by the relative timing of stimulus presentation with respect to the oscillatory cycle in visual (Kasten and Herrmann, 2020) and olfactory (Kepecs, Uchida, and Mainen, 2006; Smear et al., 2011) areas. Therefore, the rhythmic field activity observed in the brain areas comprising the sensory hierarchy seems to provide the scaffolding of sensory signals to be represented in local circuits by enabling the repeated sampling of synaptic inputs. Furthermore, an intriguing interpretation of this type of rhythmic synaptic sampling could be that it supports a probabilistic inference process of the probability distributions underlying the generation of the sensory stream (Buesing et al., 2011;

Korcsak-Gorzo et al., 2022).

Following the above reasoning, one could expect that oscillations in brain circuits have been selected by the evolutionary process to optimize information encoding and transmission. Indeed, the prominent role of oscillations in neuronal communication (Fries, 2015), together with the conservation of the basic oscillatory rhythms across animal species (Buzsáki, Logothetis, and Singer, 2013) favors such a hypothesis. However, a fundamental question is why such a low frequency range would have emerged over others that could provide increased bandwidth and sampling resolution?

In this paper, we use a computational model to study how hippocampal neurons encode information from their synaptic inputs in their spike times relative to a background field oscillation (i.e., phase code). We first analyze the response statistics of stochastic leaky integrate-and-fire neurons constrained by physiologically realistic parameters from the rodent hippocampus. Then, we propose an information-theoretical framework to estimate information rate from the neuron's phase code, which allows for the analysis of the relationship between information, oscillation frequency, and noise (i.e., random membrane fluctuations), focusing on how noise shapes the information rate profiles across frequencies. Finally, we demonstrate how our approach provides principled and optimality-based explanations to several key physiological phenomena observed in the hippocampus, such as the existence of theta-band oscillations across the entire dorsoventral axis, or the modulations of the theta oscillation properties as animals vary their locomotion speed.

2 Results

2.1 Neural model and information-theoretical framework

We first characterize the phase locking responses with deterministic, oscillation-driven dynamics in the leaky integrate-and-fire (LIF) neuron model. Subsequently, we incorporate noise and show its effects on the phase distributions of the stochastic LIF neuron driven by oscillations across a range of frequencies. We then describe the information-theoretical framework that we use to study phase coding within such a model, leading to accurate estimations of its information throughput across different noise and frequency levels.

2.1.1 Phase locking in LIF neurons with deterministic dynamics

Our LIF neuron model describes the time evolution of a neuron's membrane potential that receives both a tonic input current I_s, representing the stimulus to be sampled, and an oscillatory input current I_θ, representing periodic oscillations in the membrane potential that are caused by either the ephaptic effects of the LFP, rhythmic inhibition, or background firing rate activity (Figure 1A). Neurons following this type of dynamics enter into a phase locking mode whereby their spike time with respect to I_θ (i.e., their phase) is stably maintained across cycles. In fact, by imposing this condition in the model (i.e., a constant inter-spike interval equal to the oscillatory period T), one can obtain an analytical expression that relates the input I_s to its corresponding output phase ϕ, as well as the range of I_s for which such a phase locking is

possible (see section 4.2 in Methods):

$$\phi(I_s) = \arccos\left(\frac{V_{th}}{R_m I_{osc} A\left(1 - e^{-T/\tau_m}\right)} - \frac{I_s}{A I_{osc}}\right) - \varphi \tag{1}$$

Equation (1) represents the rate-to-phase transform and characterizes the phase locking dynamics of deterministic LIF neurons driven by oscillations, showing how the phase of the first spike per cycle advances monotonically (and non-linearly) as the input I_s is increased (Figure 1B and C), and resembling the phase precession phenomenon in the hippocampus. Indeed, the first spikes across cycles (Figure 1B, yellow dots) show that phase locking only occurs for a particular range of I_s levels –which correspond to the domain of the function given by Equation (1), see Figure 1C. Below the phase locking range, the neuron remains sub-threshold and never fires, whereas above the phase locking range, the neuron becomes asynchronous to the oscillation. It is worth noting that Equation (1) is only an approximation of the neuron's actual behavior, since the equation is only exact when there is a single spike per cycle and additional spikes break the assumption of having a constant inter-spike interval (see Figure 1C). Nonetheless, this slight discrepancy between theory and simulations does not prevent the phase locking regime to be reliably obtained across all parameters considered in this manuscript.

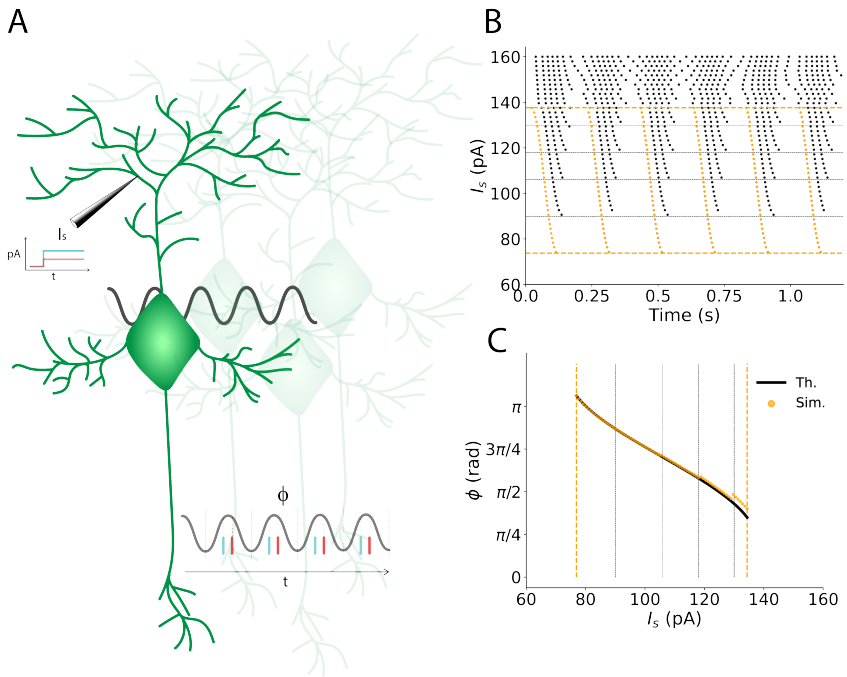

Figure 1: Oscillation-driven neurons exhibit phase locking for a range of tonic inputs. A. Response of a LIF neuron jointly driven by an oscillatory and a tonic input current. The level of tonic input determines the phase at which the neuron will spike, with stronger inputs (cyan) producing spikes at earlier phases than weaker inputs (red). **B.** Raster plot of a LIF neuron with parameters from the hippocampal pyramidal cell and driven by a 5 Hz oscillation and different levels of tonic input (as in McLelland and Paulsen (2009)). Yellow dashed lines represent the range of intensities corresponding to the phase locking regime, whereas the yellow dots denote the first spike of each cycle. Below the phase locking regime, no spikes are generated, and above it, neurons become asynchronous to the oscillation. **C.** Rate-to-phase transform (i.e., transfer function) derived from Equation (1) (solid black line). Yellow dots correspond to the phase of the first spike per cycle obtained from the simulations shown in panel B. As in panel B, dashed black and yellow lines indicate the emergence of additional spikes per cycle and the phase locking regime, respectively.

2.1.2 Spike phase distributions in LIF neurons with stochastic dynamics

In the previous section, we showed that oscillation-driven LIF neurons can implement a rate-to-phase transform that might support the kind of input sampling through phase coding observed in areas like the hippocampus. However, the dynamics considered so far have been deterministic, that is, without any source of noise. Here, we extend and generalize our analysis by considering neurons that are subjected to random fluctuations in their membrane potential (see example in Figure 2B), leading to the stochastic LIF neuron model described as (see Methods for further details):

$$\tau_m \frac{dV}{dt} = -V + R_m I_{osc} \cos(\omega t + \phi_0) + R_m I_s + \sigma_W \xi(t) \tag{2}$$

$$V(t') \geq V_{th} \Longrightarrow V(t' + \delta t) = V_{reset} \tag{3}$$

If Equation (1) provided a direct mapping between the tonic input I_s and the phase of the first spike $\phi(I_s)$, now the addition of noise to the membrane dynamics in Equation (2) adds uncertainty to this mapping, transforming $\phi(I_s)$ into a random variable that follows a particular probability distribution. Then, information theory can be used to analyze the phase distributions generated by neurons with stochastic dynamics and thus assess the reliability of the resulting phase code under different conditions (Figure 2A).

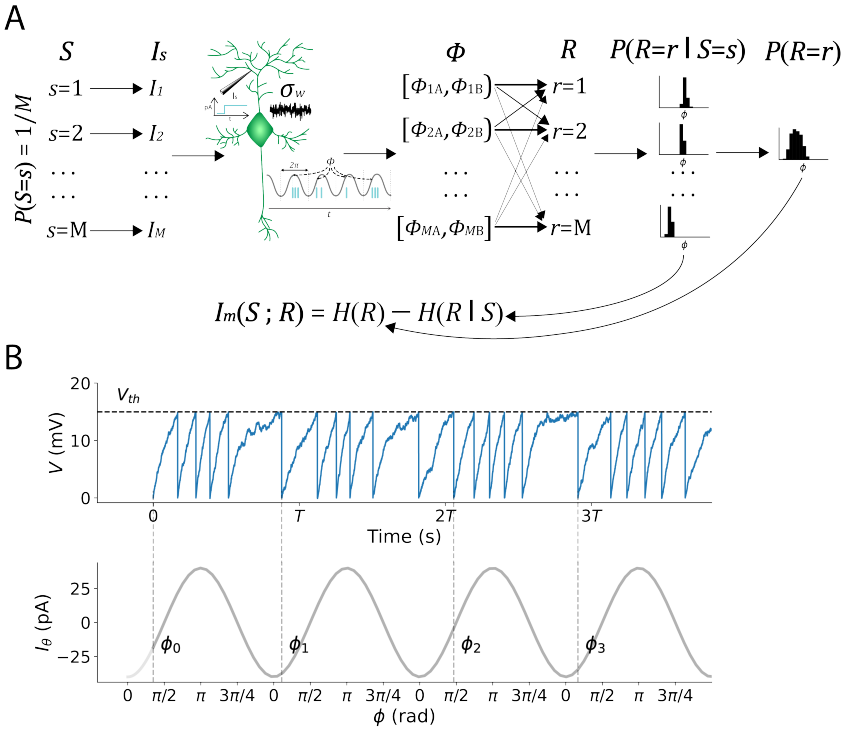

Figure 2: Phase code reliability depends on the phase distributions induced by noisy dynamics. **A.** Information-theoretical analysis of phase coding in stochastic LIF neurons. The mutual information (I_m) between a uniformly distributed stimulus s and the resulting phase ϕ can be obtained by calculating the difference in entropy between the unconditioned response (phase distribution when the stimulus is unknown, i.e., mixing across stimulus levels) and the response conditioned on the stimulus (phase distribution when the stimulus is known, i.e., holding a particular stimulus level fixed) –see Methods for further details on definitions and notation. **B.** Top: Example voltage trace of a hippocampal model neuron with parameters $f = 5$Hz, $\sigma_W = 0.01\text{V}/\sqrt{\text{s}}$ and $I_s = 134$ pA. Bottom: Oscillatory input evolution in ϕ space. Dashed lines indicate the ϕ of the neuron's first spike within each cycle (i.e., after every trough). To simulate realistic dynamics from the beginning, the neuron is initialized ($V = 0$mV) at the phase at which it would lock to under deterministic dynamics (ϕ_0), thus simulating the continuation of a recent spike.

We start by assuming that there is a uniformly distributed stimulus $S = s$ that results in a specific tonic input current I_s injected to the neuron –with the range of I_s derived from the deterministic phase locking Equation (1). Then, after simulating the neuron's behavior for long periods of time, the resulting response $R = r$ associated with the stimulus is obtained by discretizing the oscillatory phase in small, equal bins and constructing the phase histogram containing the counts of the first spikes within each oscillatory cycle (Figure 2A). In turn, the corresponding entropies of the distributions can be calculated to estimate the mutual information (I_m, in bits) between the stimulus and the response, and thus the reliability of the phase code.

Two relevant parameters that will affect the phase coding performance of the neurons are the intrinsic noise of the membrane's dynamics (σ_W) and the frequency of the oscillatory input f. Characterizing how phase is distributed is critical to understanding its success in coding an external stimulus, as different inputs leading to overlapping distributions will result in poor encoding. Therefore, we analyze the phase distributions obtained across the (f, σ_W) parameter space (Figure 3).

Examples of the phase distributions generated by different combinations of f and (σ_W) can be seen in Figure 3A. Notably, we observe that increasing f widens the phase distributions, thus increasing their variance (Figure 3A and C). Nevertheless, this widening attenuates at higher frequencies, and it is the result of different effects. On the one hand, the propagation of intrinsic noise to the variance in the phase space is heavily dependent on the steepness of the function that maps input to phase (Equation (1)), the derivative of which increases with f (see Appendix B for a more detailed analysis). On the other hand, the higher the frequency of the oscillation, the smaller its period, which results in less noise integration. This second effect is negligible for frequency values $f \leq 10$Hz. In summary, higher frequency values translate into less integrated noise, but this noise is propagated through a much steeper function (Figure 3B), so that variance in ϕ monotonically increases with f (Figure 3C). Finally, the nature of the space in which the response takes place, which is restricted to the interval $[0, 2\pi]$, imposes a hard bound on the maximum variance that these distributions can have –which would correspond to that of a uniform distribution in this interval. This hard bound also affects the means of the obtained distributions, which shift to the center of the cycle for high values of both frequency and noise (Figure 3A).

Increasing the intrinsic noise of dynamics (σ_W) also widens the obtained distributions. However, there is one exception to this, which can be observed for stronger inputs at very low frequencies (e.g., $s = 4$ and $f = 1$Hz in Figure 3B). At this frequencies, the number of spikes per cycle is high, and increasing noise produces even more additional spikes (see Figure 8C in Appendix B), which are more likely to skip the current cycle and become the first spike of the next cycle. This effect makes distributions to shift to earlier phases as noise is increased in the low-frequency range. At the same time, the variance of these distributions is also reduced due to the hard bound ($\phi = 0$) imposed by the phase space. This hard bound effect is particularly relevant for stronger inputs (e.g., $\sigma_W = 0.04$ and $f = 1$Hz in Figure 3A).

2.1.3 Mutual information in phase coding under noise

The combined effects of noise and oscillatory frequency on the resulting phase distributions (Figure 3) determine the reliability of the phase code, which is captured by the mutual infor-

mation (I_m) between the stimulus S and the neuron's response R (see Methods and Figure 2A):

$$I_m = H(R) - \mathrm{E}_s\Big[H(R|s)\Big] \tag{4}$$

With $H(R)$ as the unconditioned response (i.e., given an unknown stimulus) and $\mathrm{E}_s\Big[H(R|s)\Big]$ as the conditioned response (i.e., the expected response given a particular, known stimulus).

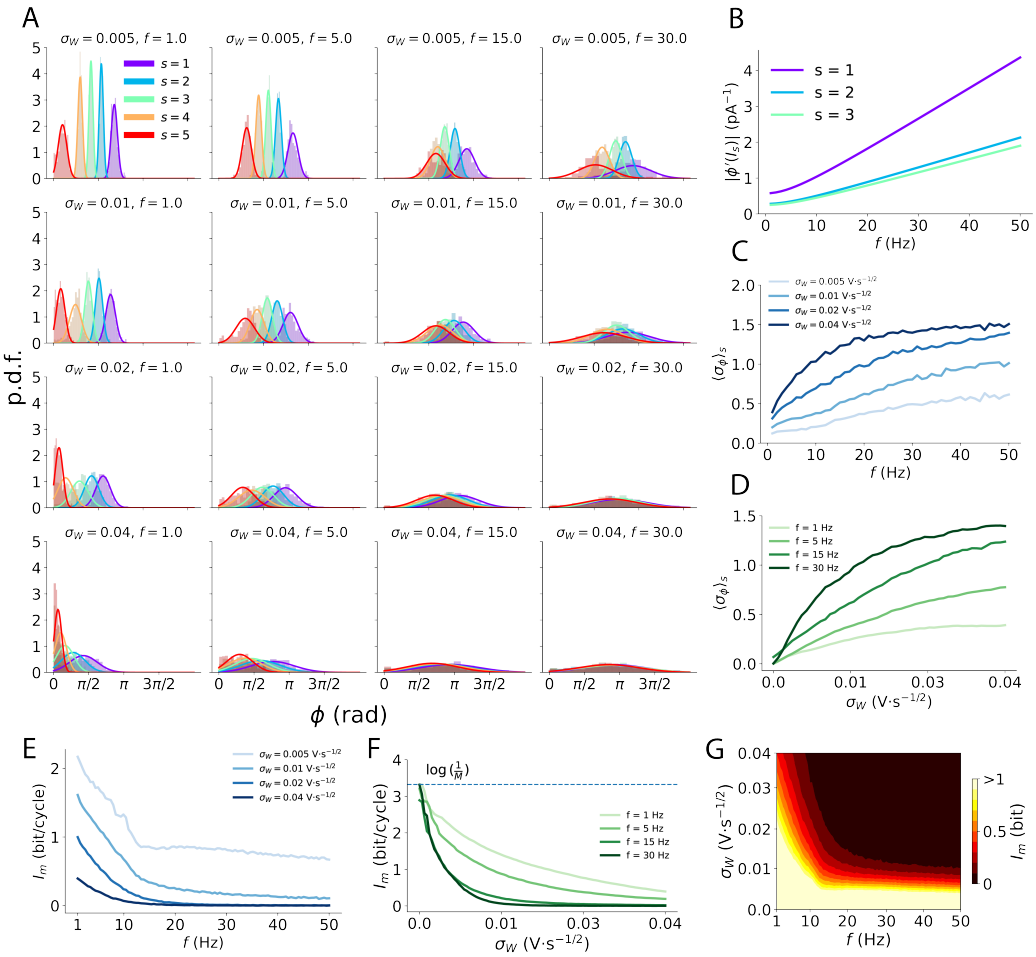

Figure 3: Phase distributions and mutual information are affected by the frequency and noise levels. A. Example phase distributions corresponding to simulations covering a wide range of the (f, σ_W) parameter space. Histograms represent the distributions of phase values conditioned on a specific stimulus level –indicated by the different colors, and starting with $s = 1$ as the weakest one. **B.** Derivative of $I_s - \phi$ curve , with $\phi'(I_s)$ as a function of frequency for increasing input levels. It indicates how steeply the noise present in input current is transferred to noise in response phase. Only the first 3 stimulus levels are shown since the profiles for $s = 4$ and $s = 5$ are identical to the one of $s = 3$. **C.** Variance in response phase as a function of frequency for increasing values of noise –with the variance being averaged across stimulus levels. **D.** Same as in panel C but fixing frequency and increasing noise. **E.** Mutual information between input and phase of first spike, derived from the corresponding phase distributions (some examples included in panel A), and as a function of frequency. **F.** Mutual information as in panel E, but as a function of noise. Dashed line indicates the upper bound on mutual information, derived from the entropy of the stimulus ($H(S)$), which follows a uniform distribution. **G.** Mutual information of phase coding across a wide range of the (f, σ_W) parameter space. Hence, it generalizes the curves shown in panels E and F. The color map is clipped at values of mutual information above 1 to prevent the extreme values in the very low-noise regime to obscure the changes in mutual information across the rest of the parameter space.

The phase distributions presented above (Figure 3A) display different mutual information profiles obtained across σ_W and f (Figure 3E, F, and G). Qualitatively, the higher the overlap

among the different conditioned responses (i.e., responses to different input levels), the more $H(R|S)$ will approach to $H(R)$, thus resulting in I_m approaching the lower bound 0. This effect is inevitable for high noise values, regardless of the magnitude of the frequency (see Methods and Figure 3F):

$$\lim_{\sigma_W \to \infty} I_m = H(R) - \lim_{\eta \to \infty} H(R|S) = H(R) - H(R) = 0 \tag{5}$$

Similarly, an upper bound on the I_m can also be computed that holds for all frequency values at zero noise ($\sigma_W = 0$):

$$\lim_{\eta \to 0} I_m = -\log\left(\frac{1}{M}\right) \underset{M=10}{\approx} 2.3 \tag{6}$$

As mentioned earlier, greater values of f result in a steeper transfer of noise from I_s to phase ϕ (Figure 2B). For this reason, the mutual information I_m decreases with increases in f for the same value of noise (Figure 2E). Nevertheless, this decrease in mutual information is not uniform across the frequency space (Figure 2F). Indeed, the I_m curves seem to converge to almost identical profiles at $f > 15$Hz (see $f = 15$Hz and $f = 30$Hz in Figure 2F). Again, we observe that this is due to the amplification of noise in ϕ with f, while the total integrated noise becomes smaller for higher values of f (i.e., shorter periods T). Therefore, there are competing effects between the integrated noise and its amplification in ϕ, as frequency is increased. Interestingly, this makes the I_m to decay towards 0 at very different rates depending on the noise level (compare ($\sigma_W = 0.005$) and ($\sigma_W = 0.01$) in Figure 3E). This introduces two regimes in the (f, σ_W) space that we will later show to be of critical relevance when considering the neurons' information rate (i.e., $R = I_m \cdot f$, in bit/s) in the context of hippocampal phase coding. In summary, in the low-noise regime, a slowly decaying $I_m \underset{f}{\rightarrow} 0$ will result in an almost ever-increasing value of R with f, whereas in the mid- or high-noise regime (which is more biologically realistic), the rapidly decaying I_m will result in a maximum of R that is confined within the low-frequency range.

2.2 Theta-band oscillations maximize the information rate in hippocampal neurons

We have demonstrated that the noise and frequency of the oscillation that shape input sampling limit the amount of information that neurons (e.g., hippocampal CA1 pyramidal cells) can convey through phase coding. Whereas noise increases the variance of phase distributions, increasing the frequency of the oscillation also tends to bring the distributions together, which enhances their overlap due to the reduction of the time window in which spikes can be emitted (Figure 4A). Therefore, it is clear that noise and frequency interact to constrain the amount of information encoded by oscillation-driven neurons following a phase code.

So far, we have referred to information as the average number of bits encoded at every cycle (i.e., mutual information I_m between the stimulus and response), which corresponds to the neurons' coding precision. However, maximizing precision requires operating at the lowest possible frequencies (see again Figure 3E and G), which implies slower timescales of input sampling and thus low reaction times. Thus, neural circuits face a fundamental speed-precision trade-off (see (Lahiri, Sohl-Dickstein, and Ganguli, 2016) for a more universal account of this trade-off in physical systems), to which a good compromise must be found that allows animals to

convey accurate sensory information while keeping up with a dynamic environment. In fact, such a speed-precision trade-off is well captured by the notion of information rate R (i.e., the expected number of bits per second). Hence, we studied this sampling-precision trade-off by estimating the R of simulated hippocampal neurons driven at different oscillatory frequencies and noise levels. By inspecting the information rate profiles at different noise levels, we observe that with

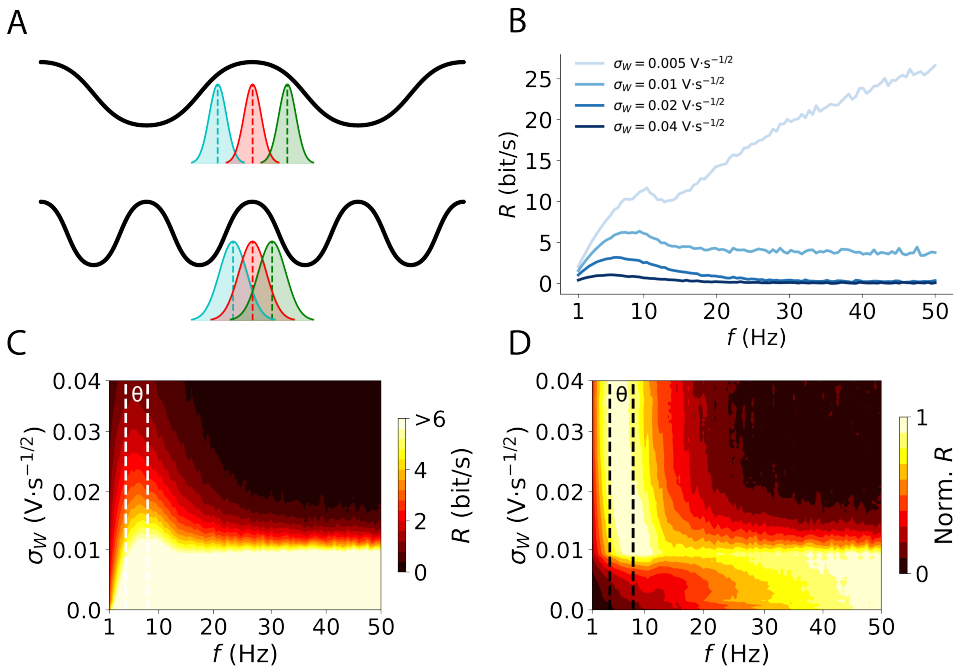

Figure 4: Speed-precision trade-off in the phase coding by hippocampal neurons. A. Effect of oscillatory frequency on phase distributions. Increasing the oscillatory frequency decreases the effective time window for firing while increasing the spike time variability, thus enhancing the overlap among phase distributions generated by different inputs or stimulus levels. **B.** Information rate (R, in bit/s) estimated by multiplying the mutual information I_m with the oscillatory frequency f. The peaks at low frequencies result from the trade-off between sampling frequency and coding precision. **C.** Generalization of panel B for a wide range of noise levels, characterizing the (f, σ_W) parameter space in terms of information rate. The color map of the R values was clipped from above at 6 bit/s to prevent the extreme values in the high frequency-low noise regime to obscuring the otherwise visible peaks within the theta band ($4 - 8$Hz, denoted by the vertical dashed lines). **D.** Normalization of the information rate in panel C with the corresponding maximum value within each noise level, with the peaks ($R = 1$) denoting the optimal frequency range at each particular level of noise considered.

low noise, the R increases without an upper bound within the range of the physiologically-relevant frequencies considered here (Figure 4B). As mentioned in the previous section, this effect is due to a very slow decay of the mutual information towards 0 that makes it to effectively plateau at values well above 0 in the considered range (see Figure 3E). However, as noise is increased, the information rate becomes overall smaller, due to the rapid decrease in coding precision (i.e., I_m), with a larger effect at higher frequencies. This steep convergence of R to 0 as a function of f leaves an information rate maximum within the low-frequency range. We can indeed observe the emergence of this maximum more clearly in Figure 4C and D, where a wider (f, σ_W) parameter space is shown. Since we are interested in finding the optimal frequency bands given a particular noise level, we normalized the information rate with its maximum value within each noise level (Figure 4D). We can now observe clearly the existence of the two noise regimes: the low-noise regime, with unbounded R with respect to f, shown by peak R values at the highest frequencies considered here; and the mid- and high-noise regime, with local R maxima within the low-frequency bands (i.e., $f < 15$Hz). Interestingly, the phase transition

between the two regimes shows that there is a critical level of noise where the speed-precision trade-off appears, and that this trade-off is optimized in the theta-frequency band for model neurons with parameters from the rodent hippocampus and under physiological noise levels (i.e., around $\sigma_W = 0.16$ V/$\sqrt{\text{second}}$ (Lansky, Sanda, and He, 2006)). Hence, these results suggest that hippocampal neurons are indeed subjected to a speed-precision trade-off and that theta oscillations provide optimal sampling capabilities.

2.3 Theta remains optimal throughout the dorsoventral axis

The circuits of the hippocampus are not homogeneous, and basic physiological properties of neurons and local circuits change consistently across its axes (Soltesz and Losonczy, 2018; Witter et al., 2000). Specifically, as we move along the dorsoventral (DV) –or septotemporal– axis, the membrane's input resistance, action potential threshold, and the membrane time constant of pyramidal cells, together with the amplitude of the local field oscillation, change in a nearly linear manner (Malik et al., 2016; Patel et al., 2012). The co-variation of these physiological properties across the DV axis displays a smooth gradient (Figure 5A, right). Interestingly, recordings of the local field potential along the entire DV axis have revealed a traveling wave in the theta band, with a total phase offset between the extreme DV poles of approximately 180°, or half a cycle (Patel et al., 2012) (Figure 5A, left). Therefore, the dominant theta frequency is maintained throughout the entire DV axis despite the gradient in physiological properties. Given that our results so far suggest that theta is the optimal frequency band for input sampling in a prototypical model of the hippocampal CA1 pyramidal cell (Figure 4), the above observations thus raise the question of whether the optimality of the theta band also holds for the entire DV axis, once more physiologically-detailed parameters are considered?

We hypothesize that it is indeed the precise co-variation of these physiological parameters what makes theta the preferred frequency across the DV axis, by optimizing the speed-accuracy trade-off in all regions. To test this hypothesis, we estimated the information rate across the DV gradient, setting the noise parameter (σ_W) at a physiologically realistic level (i.e., $\sigma_W = 0.16$ V/$\sqrt{\text{second}}$ (Lansky, Sanda, and He, 2006)). We found that the theta frequency band displays normalized information rate R peaks along the entire DV axis, thus making theta the optimal frequency band for input sampling with phase coding in all regions (Figure 5B and C).

So how can the optimality of theta be understood despite the pronounced gradient in physiological parameters? We notice that, despite the systematic variations in key parameters, the R_m/τ_m ratio remains practically constant along the DV axis. As a result, the shape of the transfer function remains equally similar (shown in Figure 4E in McLelland and Paulsen (2009)). That is, changes in the membrane time constant can be effectively compensated by proportional changes in the membrane's input resistance, thus keeping a constant R_m/τ_m ratio. In addition to this, lower amplitude oscillations in more ventral sites are also compensated by higher excitability in the form of lower action potential thresholds (Dougherty, Islam, and Johnston, 2012).

From these results, we conclude that physiological changes across the DV axis –which probably reflect different needs of input processing due to distinct afferent connectivity patterns (M.-B. Moser and E. I. Moser, 1998; Witter et al., 2000)– co-vary so that neurons along the DV axis can optimally sample their heterogeneous inputs at the same frequency.

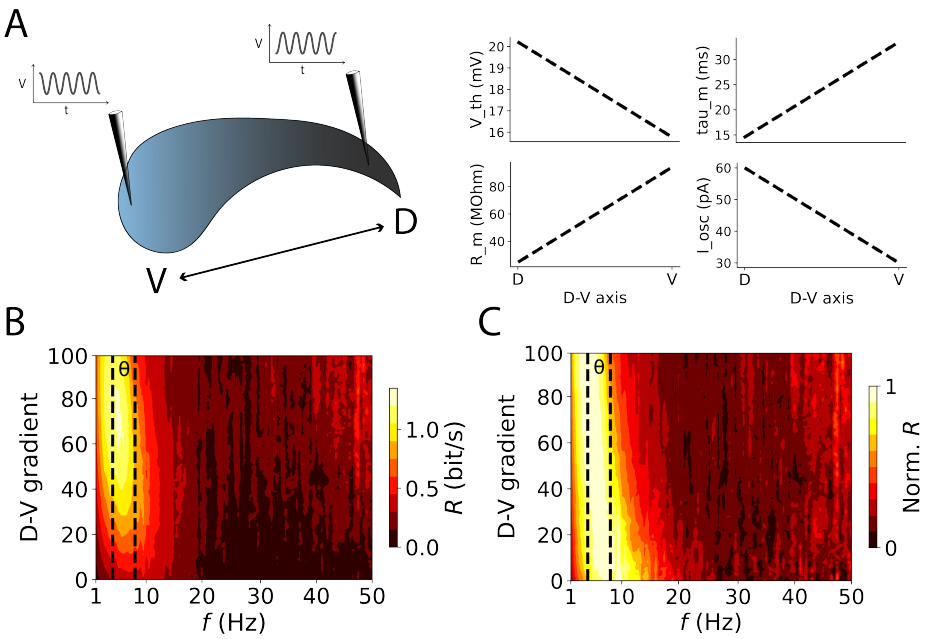

Figure 5: Physiological gradient in the dorsoventral axis of the rodent hippocampus conserves theta optimality. A. (Left) Schematic of the rodent hippocampus, denoting the dorsal and ventral poles, where the oscillation frequency is the same (around 5 Hz), but there is an offset of 180º between poles (Patel et al., 2012). (Right) Linear fits of the physiological gradients, as reported in Malik et al. (2016) for the action potential threshold, the membrane resistance at the resting potential, and the membrane time constant, and as estimated for the oscillatory amplitude of theta from Patel et al. (2012). Thus, the DV gradient is characterized by the co-variation of core physiological parameters. **B.** Information rate (R, in bit/s) along the DV axis as defined by simulated neurons following the estimated physiological gradient. The theta frequency band is denoted by the vertical dashed lines. **C.** Normalization of the R values in panel B with the corresponding maxima per DV level, with the peaks indicating the optimal frequency range at each point of the DV axis.

2.4 Optimal information rate relies on the speed-dependent modulation of theta frequency and amplitude

As animals move around the environment, they change their locomotion speed to meet internal and task demands. Running faster leads to an increased rate of change of incoming stimuli, which in turn could imply the need to increase the frequency of perceptual sampling and the associated brain rhythms to normalize memory content (Pata et al., 2022). Since theta oscillations set the pace at which the hippocampus samples, processes, and exchanges information with the entorhinal cortex, one would expect theta to be modulated by speed (Figure 6A). Indeed, shifts in theta frequency that are linearly dependent on locomotion speed have been observed in the rodent hippocampus (McFarland, Teitelbaum, and Hedges, 1975; Sławińska and Kasicki, 1998; Young, Ruan, and McNaughton, 2020), especially in dorsal sites, which receive sensory-related signals. Moreover, this theta frequency-speed dependence has been observed in humans as well, especially in the posterior (dorsal in rodents) hippocampus (Goyal et al., 2020). Therefore, hippocampal theta has been argued to modulate speed-controlled pyramidal oscillators to maintain a constant relationship between the time-varying rate inputs (place fields) and spike phase (Geisler et al., 2007). Alongside these peak frequency shifts, the amplitude (and power) of the theta rhythm has also been shown to be modulated by locomotion speed (Long, Bunce, and Chrobak, 2015; Young, Ruan, and McNaughton, 2020). Furthermore, both the frequency and amplitude seem to shift proportionally and to keep a nearly linear relationship with the animal's speed (Young, Ruan, and McNaughton, 2020). Hence, we hypothesized that

this speed-dependent concurrent modulation of frequency and amplitude of theta is a signature of information rate maximization.

To test our hypothesis, we computed the information rate R across a range of frequencies and oscillatory amplitudes (I_{osc}), with the parameters corresponding to prototypical pyramidal cells in the dorsal CA1 (see Methods). We observe a clear peak shift towards higher frequency values as the amplitude I_{osc} is increased (Figure 6B). Moreover, a nearly linear relationship between f and I_{osc} can be observed with respect to the information rate peaks, encompassing the theta band (4-8 Hz), as well as the alpha band (8-14 Hz) for higher amplitude values (Figure 6C and D). These results show that maximizing information rate necessitates the concurrent modulation of frequency and amplitude, thus explaining why both oscillatory features increase proportionally and linearly with speed.

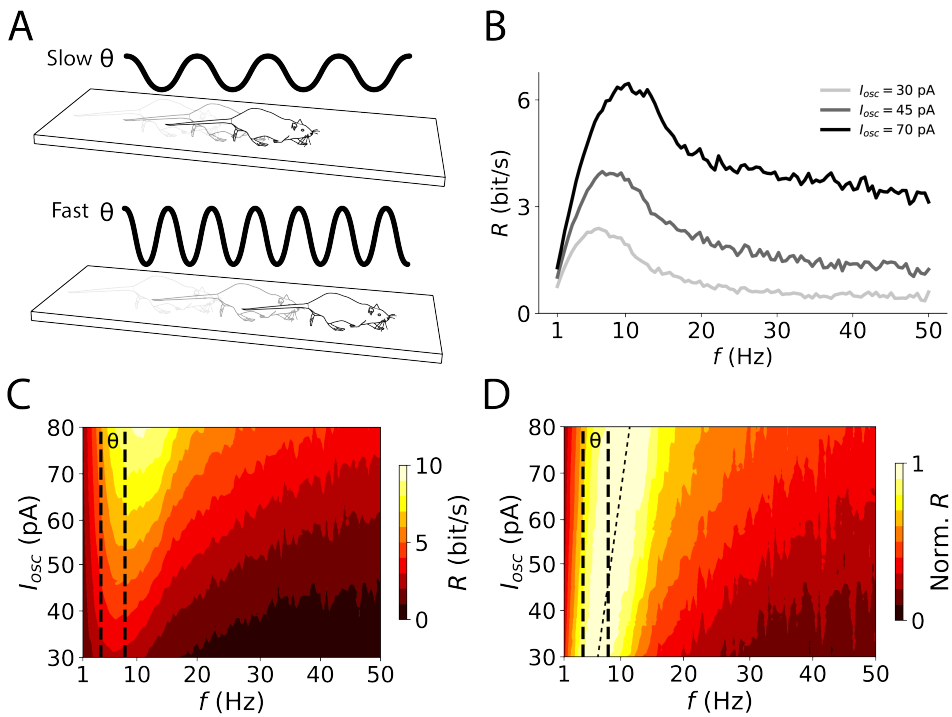

Figure 6: Locomotion speed-dependent modulation of the frequency and amplitude of the hippocampal theta rhythm as a signature of information rate maximization. A. Schematic showing how locomotion speed modulates the oscillatory frequency (f) and amplitude (I_{osc}) of theta. **B.** Information rate R (bit/s) across frequencies with different oscillation amplitudes. **C.** Generalization of panel B, showing the information rate across the (f, I_{osc}) parameter space. Vertical dashed lines indicate the theta-frequency band. **D.** Normalization of panel C with the maximum R within each amplitude level, showing the nearly linear relationship (thin dashed line) between frequency and amplitude with respect to the optimal information rate.

3 Discussion

We have studied the relationship between sampling speed and coding precision of phase coding in simulated hippocampal cells. We have approximated the physiology of the hippocampus with stochastic LIF neurons that receive combined tonic and oscillatory inputs, with the former encoding an external stimulus and the latter emulating the rhythmic excitability changes caused by local oscillatory effects. From a phase coding perspective, the oscillation could serve as an input sampling mechanism, with the spike times in each cycle representing one sample that

is drawn from the probability distribution underlying the external (synaptic) input (Buesing et al., 2011; Korcsak-Gorzo et al., 2022). Hence, we quantified the amount of information contained in a neuron's firing time (i.e., phase) while being subjected to varying levels of random fluctuations of the membrane potential (i.e., noise). In other words, we studied how reliably a hippocampal CA1 neuron can map different levels of tonic input to precise spike times (i.e., rate-to-phase transform) in the presence of noise. By assuming statistical independence across oscillatory cycles, we could estimate the information rate (bits per second) of these neurons for a wide range of noise and oscillatory frequency values. We identified that under physiologically relevant conditions, low-frequency oscillations in the theta band provide optimal rate of phase coding –and thus optimal input sampling.

3.1 Speed-precision trade-off and information rate maximization in neural sampling

Firing rate inputs to a neural circuit can be efficiently sampled, encoded, and conveyed to downstream neurons by a rate-to-phase transform that is enabled by an oscillation. However, random fluctuations generated by the massive synaptic bombardment that neurons receive constrain how reliably the firing rate input can be mapped into such a temporal or phase code. In addition, high-frequency oscillations, which in principle could provide fast input sampling, reduce the time window for neurons to integrate and emit a spike, effectively hampering the precision of the input-output transformation as well. Therefore, noise and oscillatory frequency interact to determine the amount of phase-coded information in a particular neural circuit. Here, we identified a trade-off between coding precision (bits per cycle) and sampling frequency (cycles per second) that appears beyond a critical level of noise (Figure 4). This speed-precision trade-off is optimized at the theta frequency band (4-8 Hz) for hippocampal CA1 neurons (Figure 4D and Figure 5C)), suggesting that single cell properties and oscillation frequency in the hippocampus are jointly tuned to maximize information rate of phase coding under physiological levels of noise. The above observation applies mainly to the CA1 subfield of the hippocampus, which is the one directly receiving and encoding sensory inputs from the superficial layers of the entorhinal cortex, making CA1 neurons to phase precess across the first half of the theta cycle (Guardamagna, Stella, and Battaglia, 2021), also consistent with the phase distributions reported here (e.g., $\sigma_W = 0.02$ and $f = 5$Hz in Figure 3A).

Our observation that theta oscillations yield optimal information rate in a model of hippocampal neurons raises the question of how single cell properties constrain the optimal region within the parameter space determined by the frequency and noise levels. This type of analysis opens the possibility to explore the relationship between single cell properties and local oscillations in other brain areas or species, including humans. For instance, the human hippocampus is dominated by two distinct theta rhythms (Goyal et al., 2020), which might imply both the existence of two qualitatively different types of pyramidal neurons with different properties (e.g., membrane time constants) as well as two low-frequency phase coding channels. Similarly, phase coding has been hypothesized to take place in a number of species and neural systems, including the rodent olfactory bulb (Margrie and Schaefer, 2003) and the primate visual cortex (Montemurro et al., 2008) (see also (Caplette, Jerbi, and Gosselin, 2022) for an example of rhythmic sampling in the visual system). Further, given our results, we can now map the single cell properties of these brain areas to the frequencies that optimize phase-coded information

rate and thus evaluate the plausibility that such a coding scheme is being employed by the corresponding local circuits.

3.2 Theta waves, computation, and gradients across the dorsoventral axis

We showed that theta remains the optimal frequency band across the entire dorsoventral axis of the hippocampus. This maximization of information rate provides a plausible explanation to why theta is maintained as the dominant frequency in the hippocampus despite the pronounced gradients of single cell properties throughout this axis. Maintaining the same frequency throughout the DV axis could allow the integration and transfer of information across different levels of resolution and spatial scales (Kjelstrup et al., 2008), while serving as a uniform readout mechanism. This phase-based representation format could be further enabled by dorsoventral travelling waves that are known to follow the DV axis (Patel et al., 2012). In parallel, different regions across the DV axis might need to process inputs from different modalities and with varying statistics, from slow olfactory signals to fast auditory ones. Hence, the theta-grounded phase code allows the variation of single cell properties along the DV axis to be locally tuned to diverse inputs while integrating them in a generic coding format. It should also be noted that there are other physiological gradients that we have not taken into account and that affect excitability and resonance of neurons in the hippocampus (e.g., density of HCN ion channels (Marcelin et al., 2012) or Kv7 channels (Hönigsperger et al., 2015)). However, we predict that these features further contribute to the optimality of theta oscillations. For instance, both HCN and Kv7 channels are known to promote resonant behavior of the membrane potential of CA1 pyramidal cells at around 4-5 Hz (Hönigsperger et al., 2015; Marcelin et al., 2012). Thus, we suggest that the dorsoventral gradients define a high-dimensional manifold in the space of single cell properties whereby theta remains optimal in terms of information rate, while being properly suited to process particular input statistics in a region-dependent manner, rendering a standardized and multiplexed encoding.

3.3 Speed-controlled oscillators for optimal sampling

Following earlier proposals (J. E. Lisman and Jensen, 2013), we suggest that hippocampal circuits are tuned for a phase code that is standardized to theta as a carrier wave. Under the perspective of theta oscillations as sampling, we can speculate that this theta carrier wave is in turn modulated to continuously optimize information rate. Indeed, theta fluctuates with the animal's locomotion speed (McFarland, Teitelbaum, and Hedges, 1975; Sławińska and Kasicki, 1998; Young, Ruan, and McNaughton, 2020). It has been proposed that this is due to higher cue densities in the environment leading to the upmodulation of the theta frequency to keep up with the rate of stimulus change as well as to normalize the information content per theta cycle (Pata et al., 2022). Normalizing the amount of information per theta cycle might allow downstream readers to keep constant decoding mechanisms (e.g., constant temporal offset between coherent oscillations for phase decoding (Jensen, 2001)). This normalization mechanism would prevent having continuous synaptic adaptation during varying locomotion speed, which could alter neural dynamics and destabilize the circuits. However, once single cell properties have been optimized for a particular oscillatory frequency range, substantial increases in frequency to speed up input sampling could indeed yield suboptimal information rates. We showed that a way to counteract this without resorting to modulations of single cell properties is to concurrently –

and proportionally– increase the amplitude of the oscillation, since this allows the neurons to maintain themselves within the optimal phase coding regime (Figure 6D). Indeed, we found a near-linear relationship between the optimal frequency and a given amplitude within the low-frequency range (1-15 Hz). In other words, frequency and amplitude have to vary proportionally and in a coordinated manner to maintain the phase coding by hippocampal neurons in an optimal information rate regime.

The coupling between locomotion speed, theta frequency, and amplitude raises the question of how they can be coordinated. On the one hand, the medial septum is thought to be the main driver of the theta oscillations in the hippocampus (Buzsáki, 2002; Petsche, Stumpf, and Gogolak, 1962; Pignatelli, Beyeler, and Leinekugel, 2012), while controlling locomotion speed and hippocampal theta frequency (Fuhrmann et al., 2015; Tsanov, 2017). On the other hand, the cooling of the medial septum slows down the hippocampal theta rhythm while leaving the neurons' phase relationships intact, hence preserving the phase code under the alteration of the oscillatory frequency (Petersen and Buzsáki, 2020). This suggests that a possible normalizing mechanism underlying the linear, proportional modulation of frequency and amplitude of the theta rhythm in the hippocampus might be an input-driven global oscillator in the medial septum, which would also modulate the oscillatory frequency of the local oscillators (Fuhrmann et al., 2015; Goutagny, Jackson, and Williams, 2009). The net input (i.e., time-varying firing rate) would in turn be the key driver of such oscillations, which is indeed consistent with the observed Huygens synchronization of medial septum's pacemaker neurons (Kocsis et al., 2022).

3.4 Limitations and future work

The information-theoretical approach to neuronal sampling implies the existence of downstream decoding mechanisms that perform the readout of the information encoded by the phase of firing. Therefore, the binning of phase leading to discrete phase distributions that are in turn used to compute the mutual information imposes a minimal temporal resolution at which the decoder is assumed to operate. Here we used a resolution of 10 phase bins per cycle, which corresponds to 2ms bins for the maximum frequency considered (i.e., 50Hz), and 100ms bins for the minimum frequency (i.e., 1Hz). However, extensive simulations reveal that improving the temporal resolution in the low-frequency regime (i.e., using 2ms bins across all frequencies) does not affect significantly the estimation of the mutual information (data not shown). This observation seems to be in agreement with previous physiological studies that showed that discretizing the hippocampal theta cycle in only three bins was enough to accurately reconstruct the animal's position in space (Jensen and J. E. Lisman, 2000). This suggests that the hippocampal phase code might not need high temporal resolution to support behaviorally-relevant functions like spatial navigation. Moreover, the modulation of pyramidal cell activity by theta-nested gamma oscillations produced by fast-spiking interneurons in the hipppocampus (J. E. Lisman and Jensen, 2013) further constrains the number of effective phase bins (or time slots) that could be available for decoding, given that spikes tend to be clustered around the 5 to 10 gamma cycles at each theta cycle. This coarse discretization would allow robust decoding by maintaining stable phase offsets between oscillations in different neural circuits (Jensen, 2001). Indeed, systematic phase offsets between circuits could be maintained by a robust travelling wave such as the one observed in the hippocampus (Patel et al., 2012). Therefore, more work is needed to understand the precise relationship between the biophysical constraints and the

variety of decoding mechanisms imposed by temporal codes in different brain regions.

One of the key assumptions that the framework of oscillations as neural sampling makes is that each cycle represents an independent sample of the underlying input distribution. Indeed, this is reflected in our estimation of the information rate, that is computed by multiplying the mutual information between input and output per cycle with the number of cycles per second (i.e., frequency). However, this assumption of statistical independence between oscillatory cycles might be violated in the case of temporal correlations (see (Knüsel et al., 2004)), either because no proper reset can be performed after every cycle (e.g., due to slow membrane time constants), or because the oscillation frequency is higher than the expected rate of change in the input signal (i.e., leading to oversampling). Hence, the leakage of redundant information across cycles makes our estimation of the information rate an upper bound on the actual information rate. However, it is worth noting that this loss of information rate due to temporal correlations becomes more prominent with higher frequencies (i.e., >20Hz), which lie above the physiologically-relevant range for the hippocampus (1-15Hz). However, it remains to be answered whether the characteristic time constant of the firing rate input from the entorhinal cortex to the hippocampal CA1 matches the theta-frequency timescale of the hippocampus.

Although here we focused on neural sampling through phase coding, it is likely that the brain uses different codes across different regions (e.g., instantaneous firing rates, bursts, inter-spike intervals, etc.), sometimes even multiplexing them in the same network of neurons (Huxter, Burgess, and O'Keefe, 2003; Naud and Sprekeler, 2018). For example, neurons receiving direct input from receptor cells are typically thought to rely on a rate code that directly represents an external magnitude, e.g., light intensity (Hubel and Wiesel, 1962). Understanding the effect of oscillations in spike counts or firing rate coding could shed some light on the relevant physiological constraints and the information-theoretical quantities that are being optimized in different circuits. Indeed, we speculate that a particular relationship might exist between the information rate maximization proposed here, and the efficient coding hypothesis (Barlow et al., 1961; Park and Pillow, 2020) –e.g., by taking into account the metabolic cost of spikes together with the bits per spike. In addition, including theta-gamma nested oscillations could enable powerful combinatorial codes that go beyond simple phase coding (Buzsáki, 2010), as well as an enhanced coding precision due to theta-modulated gamma, whose fast inhibitory feedback is known to discretize the phase space (J. E. Lisman and Jensen, 2013).

Finally, we note here that our analysis of information rate is not necessarily constrained to the single cell level. Indeed, population codes likely play a key role in hippocampal information processing (Averbeck, Latham, and Pouget, 2006). Therefore, ensemble statistics could be derived from analytical approximations of single-cell phase distributions, and thus information rate estimations could account for population-level representations. This approach could clarify the role of neural ensembles in phase coding during memory-related processes. Furthermore, studying how phase-coded information can be reliably conveyed across the entire hippocampus with minimal loss (Kumar, Rotter, and Aertsen, 2010) might shed some light on the learnability of network-level representations and the overall dynamics of the trisynaptic loop, where cortical states are compressed to form memories (Santos-Pata et al., 2021a,b).

4 Materials and Methods

4.1 Deterministic neuron model

We model pyramidal cells as Leaky Integrate-and-Fire (LIF) neurons that receive inhomogeneous oscillatory input (Burkitt, 2006) and tonic synaptic input. This allows us to account for several physiological properties: (i) the passive properties of the subthreshold membrane potential, (ii) the periodic oscillations that neurons experience in many brain regions (Buzsáki and Draguhn, 2004), and (iii) the discrete nature of spike times and the subsequent potential reset. The dynamics of the membrane potential are given by the following equations:

$$\tau_m \frac{dV}{dt} = -(V - V_{rest}) + R_m I_s + R_m I_\theta \tag{7}$$

$$V(t' + dt) = V_{reset} \;\text{ if }\; V(t') = V_{th} \tag{8}$$

where V is the neuron's membrane potential, V_{rest} is the resting potential, R_m is the membrane resistance, I_θ is an oscillatory current and I_s is a tonic input current that depends on some external stimulus. The oscillatory current is parameterized as follows:

$$I_\theta = I_{osc} \cos(\omega t - \pi + \phi_0) \;\;,\;\; \omega = 2\pi f \tag{9}$$

with I_{osc} being the amplitude of the oscillation, ω and f the angular and temporal frequencies, respectively, and ϕ_0 the phase in the initial conditions. The $-\pi$ term is added for simplicity, so that $\phi_0 = 0$ and $\phi_0 = 2\pi$ correspond to the trough of the oscillation. In practice, and throughout the rest of the section, we take $V_{rest} = V_{reset} = 0$ mV.

4.2 Phase of firing

The voltage trajectory, provided a spike at time t', can be found to be (Appendix A):

$$V(t) = R_m I_s \Big(1 - e^{-(t-t')/\tau_m}\Big) + R_m I_{osc} A \Big(\cos(\omega t + \varphi + \phi_0) - e^{-(t-t')/\tau_m} \cos(\omega t' + \varphi + \phi_0) \Big) \tag{10}$$

$$\varphi = -\arctan(\omega \tau_m) - \pi \tag{11}$$

$$A = \frac{1}{\sqrt{1 + (\tau_m \omega)^2}} \tag{12}$$

The *spike phase* of a neuron in a cycle i is defined as the modulo 2π of the time of the first spike within the cycle (i.e., since the last trough), multiplied by the angular frequency ω:

$$\phi_i = \Big[\omega t_i^{(0)} \;\bmod\; 2\pi\Big] + \phi_0 \tag{13}$$

Imposing $t - t' = t_i^{(0)} - t_{i-1}^{(0)} = T \Longrightarrow t = t_0^{(i-1)} + T$, and substituting $\omega t_i^{(0)} = \phi_i - \phi_0$ in Equation 10, we obtain

$$V_{th} = \Big(R_m I_s + R_m I_{osc} A \cos(\phi_i + \varphi)\Big)\Big(1 - e^{-T/\tau_m}\Big) \tag{14}$$

Table 1: Neuron model parameters

Parameter	Description	Values	Units
V_{th}	Voltage threshold	15	mV
V_{rest}	Resting potential	0	mV
V_{reset}	Reset potential	0	mV
R_m	Membrane resistance	142	MOhm
τ_m	Membrane time constant	24	ms
η	Noise parameter	[0.05, 0.5]	p.d.u.
σ	White noise standard deviation	[0.005, 0.05]	$\mathrm{V}/\sqrt{\mathrm{s}}$
f	Oscillation temporal frequency	[1, 50]	Hz
ω	Oscillation angular frequency	[2π, 200π]	rad/s
I_{osc}	Oscillation amplitude	[40, 80]	pA
I_s	Stimulus input current	[100, 1000]	pA

where ϕ_i can be isolated:

$$\phi_i = \arccos\left(\frac{V_{th}}{R_m I_{osc} A\left(1 - e^{-T/\tau_m}\right)} - \frac{I_s}{A I_{osc}}\right) - \varphi \equiv \phi_0 \tag{15}$$

which gives the phase at which the neurons will lock to. We always initialize the neurons by setting the initial membrane potential V_0 at 0 and ϕ_0 at the phase locking value given by equation (15), so the neurons are phase locked at the initial conditions.

4.3 Stochastic neuron model

To account for the noisy nature of the received synaptic input and its integration in the soma, we add a stochastic term to equation 7:

$$\tau_m \frac{dV}{dt} = -(V - V_{rest}) + R_m I_\theta + R_m I_s + \tau_m \sigma_W \xi(t) \tag{16}$$

The last term represents additive white noise, which is defined as the formal derivative of a Wiener process: $\xi(t) \equiv dW(t)/dt$, with σ_W being:

$$\sigma_W = \eta \frac{(V_{th} - V_{rest})}{\sqrt{\tau_m}} \tag{17}$$

with η as a model parameter that determines the strength of the noise. It should be noted that σ_W has dimensions $[\mathrm{V}/\sqrt{\mathrm{second}}]$. The different parameters and values ranges used in this manuscript, together with their units, can be found in Table 1.

4.4 Estimation of the information rate

In order to evaluate the reliability of the phase coding scheme, we first need to define the phase as the response R that is associated with a stimulus S, both of which follow a certain probability distribution. Then, the mutual information I_m between S and R can be quantified in terms of the entropy of the *unconditioned* and *conditioned* response (i.e., the distribution that the

response follows when the stimulus is either unknown or fixed, respectively):

$$I_m = H(R) - \mathrm{E}_s\Big[H(R|s)\Big] \tag{18}$$

Therefore, we characterize the information contained in phase as the mutual information between the stimulus $S = s$ (which has an associated current I_s) and the phase response $R = r$. In order to estimate the mutual information between S and R, a distribution on S needs to be imposed. We will consider here that, over time, all input levels are equally likely and relevant, hence defining S as a uniformly distributed variable:

$$p(S = s) = \frac{1}{M} \tag{19}$$

This allows us to rewrite Equation (18) in the following form:

$$I_m = H(R) - \frac{1}{M}\sum_s H(R|s) \tag{20}$$

The conditioned and unconditioned response probabilities are obtained as follows:

1. For each pair (σ_W, f), we simulate the neuron's activity and obtain the minimum and maximum phases:
$$\phi_{\mathrm{MIN}} = \min(\{[\phi]_s\}) \ \ , \ \ \phi_{\mathrm{MAX}} = \max(\{[\phi]_s\}) \tag{21}$$

2. The interval $[\phi_{\mathrm{MIN}}, \phi_{\mathrm{MAX}}]$ is discretized into M bins of equal width $\Delta\phi$ with limits ϕ_{jA} and ϕ_{jB}:
$$\Big[\phi_{jA}, \phi_{jB}\Big] = \Big[\phi_{\mathrm{MIN}} + (j-1)\Delta\phi, \phi_{\mathrm{MIN}} + j\Delta\phi\Big] \tag{22}$$
$$\Delta\phi = \frac{\phi_{\mathrm{MAX}} - \phi_{\mathrm{MIN}}}{M} \tag{23}$$

3. The probability of response $j \in \{1, 2, ..., M\}$ conditioned by the stimulus $i = s$ is then:
$$p_{ij} = \frac{\#(\phi) \in [\phi]_s \ / \ \phi_{jA} \leq \phi < \phi_{jB}}{\#(\phi) \in [\phi]_s} \tag{24}$$

4. The unconditioned probability of response p_j is obtained by randomly mixing the M arrays $[\phi]_s$ into M arrays $[\phi]_s^{\mathrm{R}}$, applying Equation (24) to obtain the values p_{ij}^{R}, and then averaging over i:
$$p_j = \frac{1}{M}\sum_i p_{ij}^{\mathrm{R}} \tag{25}$$

In the limit $\sigma_W \to 0$, given a stimulus s (and thus an input current I_s), the dynamics can be considered deterministic and the response is a Dirac delta centered around the solution given by Equation (15). The entropy of the conditioned response is 0 and the sum in Equation (20) becomes 0 too. On the other hand, the unconditioned distribution follows a discrete uniform distribution, which thus has the same entropy as S.

$$\lim_{\eta \to 0} I_m = H(S) = \sum_s p_s \log(p_s) = \log\left(\frac{1}{M}\right) \tag{26}$$

In the limit $\eta \to \infty$, the response decouples from the input and:

$$\lim_{\eta\to\infty} I_m = H(R) - \lim_{\eta\to\infty} H(R|S) = H(R) - H(R) = 0 \tag{27}$$

hence losing all the information.

Finally, to estimate the information rate, we multiply the mutual information by the number of cycles (i.e., f):

$$R = I_m f \tag{28}$$

It should be noted that in doing so, we assume statistical independence between oscillatory cycles and thus the estimated information rate is in fact an upper bound on the actual information rate. However, this assumption mostly affects the information rates at frequencies that are above the low-frequency regime considered here for the hippocampus (>20Hz), and therefore it does not change the main conclusions of this study.

4.5 Simulations

We use BRIAN2 (Stimberg, Brette, and Goodman, 2019) to simulate neurons with the dynamics given by Equation (16) and parameters as shown in Table 1. Due to the stochastic nature of our equations, we use the Euler-Maruyama integration method (Kloeden and Platen, 1992). For each pair in the (σ_W, f) parameter space, 10 independent runs are simulated for 150 oscillatory cycles (thus with the total time being determined by f). Then, the phase distributions are obtained to compute I_m and R as described above.

Code Availability

The code and data to reproduce all the Figures can be found at https://github.com/adriamilcar/Optimal-Phase-Coding-in-the-Hippocampus

5 Acknowledgements

This work was supported by a HORIZON-EIC-2021 Pathfinder Challenges grant to CAVAA (project number 101071178).

References

Anastassiou, Costas A et al. (2011). "Ephaptic coupling of cortical neurons". In: *Nature neuroscience* 14.2, pp. 217–223.

Averbeck, Bruno B, Peter E Latham, and Alexandre Pouget (2006). "Neural correlations, population coding and computation". In: *Nature reviews neuroscience* 7.5, pp. 358–366.

Barlow, Horace B et al. (1961). "Possible principles underlying the transformation of sensory messages". In: *Sensory communication* 1.01.

Buesing, Lars et al. (2011). "Neural dynamics as sampling: a model for stochastic computation in recurrent networks of spiking neurons". In: *PLoS computational biology* 7.11, e1002211.

Burkitt, Anthony N (2006). "A review of the integrate-and-fire neuron model: II. Inhomogeneous synaptic input and network properties". In: *Biological cybernetics* 95.2, pp. 97–112.

Buzsáki, György (2002). "Theta oscillations in the hippocampus". In: *Neuron* 33.3, pp. 325–340.

Buzsáki, György (2010). “Neural syntax: cell assemblies, synapsembles, and readers”. In: *Neuron* 68.3, pp. 362–385.

Buzsáki, György and Andreas Draguhn (2004). “Neuronal oscillations in cortical networks”. In: *science* 304.5679, pp. 1926–1929.

Buzsáki, György, Nikos Logothetis, and Wolf Singer (2013). “Scaling brain size, keeping timing: evolutionary preservation of brain rhythms”. In: *Neuron* 80.3, pp. 751–764.

Caplette, Laurent, Karim Jerbi, and Frédéric Gosselin (2022). “Rhythmic information sampling in the brain during visual recognition”. In: *bioRxiv*.

Dougherty, Kelly A, Tasnim Islam, and Daniel Johnston (2012). “Intrinsic excitability of CA1 pyramidal neurones from the rat dorsal and ventral hippocampus”. In: *The Journal of physiology* 590.22, pp. 5707–5722.

Fries, Pascal (2015). “Rhythms for cognition: communication through coherence”. In: *Neuron* 88.1, pp. 220–235.

Fuhrmann, Falko et al. (2015). “Locomotion, theta oscillations, and the speed-correlated firing of hippocampal neurons are controlled by a medial septal glutamatergic circuit”. In: *Neuron* 86.5, pp. 1253–1264.

Geisler, Caroline et al. (2007). “Hippocampal place cell assemblies are speed-controlled oscillators”. In: *Proceedings of the National Academy of Sciences* 104.19, pp. 8149–8154.

Goutagny, Romain, Jesse Jackson, and Sylvain Williams (2009). “Self-generated theta oscillations in the hippocampus”. In: *Nature neuroscience* 12.12, pp. 1491–1493.

Goyal, Abhinav et al. (2020). “Functionally distinct high and low theta oscillations in the human hippocampus”. In: *Nature communications* 11.1, pp. 1–10.

Guardamagna, Matteo, Federico Stella, and Francesco P Battaglia (2021). “Distinct hippocampal network states support theta phase precession and theta sequences in CA1”. In: *bioRxiv*.

Hönigsperger, Christoph et al. (2015). “Dorsoventral differences in Kv7/M-current and its impact on resonance, temporal summation and excitability in rat hippocampal pyramidal cells”. In: *The Journal of physiology* 593.7, pp. 1551–1580.

Hubel, David H and Torsten N Wiesel (1962). “Receptive fields, binocular interaction and functional architecture in the cat’s visual cortex”. In: *The Journal of physiology* 160.1, pp. 106–154.

Huxter, John, Neil Burgess, and John O’Keefe (2003). “Independent rate and temporal coding in hippocampal pyramidal cells”. In: *Nature* 425.6960, pp. 828–832.

Jensen, Ole (2001). “Information transfer between rhythmically coupled networks: reading the hippocampal phase code”. In: *Neural computation* 13.12, pp. 2743–2761.

Jensen, Ole and John E Lisman (2000). “Position reconstruction from an ensemble of hippocampal place cells: contribution of theta phase coding”. In: *Journal of neurophysiology* 83.5, pp. 2602–2609.

Kasten, Florian H and Christoph S Herrmann (2020). “Discrete sampling in perception via neuronal oscillations—Evidence from rhythmic, non-invasive brain stimulation”. In: *European Journal of Neuroscience*.

Kepecs, Adam, Naoshige Uchida, and Zachary F Mainen (2006). “The sniff as a unit of olfactory processing”. In: *Chemical senses* 31.2, pp. 167–179.

Kjelstrup, Kirsten Brun et al. (2008). “Finite scale of spatial representation in the hippocampus”. In: *Science* 321.5885, pp. 140–143.

Kloeden, Peter E and Eckhard Platen (1992). “Stochastic differential equations”. In: *Numerical solution of stochastic differential equations*. Springer, pp. 103–160.

Knüsel, Philipp et al. (2004). “Decoding a temporal population code”. In: *Neural computation* 16.10, pp. 2079–2100.

Kocsis, Barnabás et al. (2022). “Huygens synchronization of medial septal pacemaker neurons generates hippocampal theta oscillation”. In: *Cell Reports* 40.5, p. 111149.

Korcsak-Gorzo, Agnes et al. (2022). "Cortical oscillations support sampling-based computations in spiking neural networks". In: *PLoS computational biology* 18.3, e1009753.

Kumar, Arvind, Stefan Rotter, and Ad Aertsen (2010). "Spiking activity propagation in neuronal networks: reconciling different perspectives on neural coding". In: *Nature reviews neuroscience* 11.9, pp. 615–627.

Lahiri, Subhaneil, Jascha Sohl-Dickstein, and Surya Ganguli (2016). "A universal tradeoff between power, precision and speed in physical communication". In: *arXiv preprint arXiv:1603.07758*.

Lansky, Petr, Pavel Sanda, and Jufang He (2006). "The parameters of the stochastic leaky integrate-and-fire neuronal model". In: *Journal of Computational Neuroscience* 21.2, pp. 211–223.

Lisman, John (2005). "The theta/gamma discrete phase code occuring during the hippocampal phase precession may be a more general brain coding scheme". In: *Hippocampus* 15.7, pp. 913–922.

Lisman, John E and Ole Jensen (2013). "The theta-gamma neural code". In: *Neuron* 77.6, pp. 1002–1016.

Long, Lauren L, Jamie G Bunce, and James J Chrobak (2015). "Theta variation and spatiotemporal scaling along the septotemporal axis of the hippocampus". In: *Frontiers in systems neuroscience* 9, p. 37.

Malik, Ruchi et al. (2016). "Mapping the electrophysiological and morphological properties of CA 1 pyramidal neurons along the longitudinal hippocampal axis". In: *Hippocampus* 26.3, pp. 341–361.

Marcelin, Béatrice et al. (2012). "Dorsoventral differences in intrinsic properties in developing CA1 pyramidal cells". In: *Journal of Neuroscience* 32.11, pp. 3736–3747.

Margrie, Troy W and Andreas T Schaefer (2003). "Theta oscillation coupled spike latencies yield computational vigour in a mammalian sensory system". In: *The Journal of physiology* 546.2, pp. 363–374.

McFarland, Willard L, Herman Teitelbaum, and Elizabeth K Hedges (1975). "Relationship between hippocampal theta activity and running speed in the rat." In: *Journal of comparative and physiological psychology* 88.1, p. 324.

McLelland, Douglas and Ole Paulsen (2009). "Neuronal oscillations and the rate-to-phase transform: mechanism, model and mutual information". In: *The Journal of physiology* 587.4, pp. 769–785.

Mehta, MR, AK Lee, and MA Wilson (2002). "Role of experience and oscillations in transforming a rate code into a temporal code". In: *Nature* 417.6890, pp. 741–746.

Mizuseki, Kenji et al. (2009). "Theta oscillations provide temporal windows for local circuit computation in the entorhinal-hippocampal loop". In: *Neuron* 64.2, pp. 267–280.

Montemurro, Marcelo A et al. (2008). "Phase-of-firing coding of natural visual stimuli in primary visual cortex". In: *Current biology* 18.5, pp. 375–380.

Moser, May-Britt and Edvard I Moser (1998). "Functional differentiation in the hippocampus". In: *Hippocampus* 8.6, pp. 608–619.

Naud, Richard and Henning Sprekeler (2018). "Sparse bursts optimize information transmission in a multiplexed neural code". In: *Proceedings of the National Academy of Sciences* 115.27, E6329–E6338.

O'Keefe, John and Michael L Recce (1993). "Phase relationship between hippocampal place units and the EEG theta rhythm". In: *Hippocampus* 3.3, pp. 317–330.

Park, Il Memming and Jonathan W Pillow (2020). "Bayesian efficient coding". In: *BioRxiv*, p. 178418.

Pata, Diogo et al. (2022). "Theta oscillations in the human hippocampus normalize the information content of episodic memory". In: *bioRxiv*.

Patel, Jagdish et al. (2012). "Traveling theta waves along the entire septotemporal axis of the hippocampus". In: *Neuron* 75.3, pp. 410–417.

Petersen, Peter Christian and György Buzsáki (2020). "Cooling of medial septum reveals theta phase lag coordination of hippocampal cell assemblies". In: *Neuron* 107.4, pp. 731–744.

Petsche, H, Ch Stumpf, and G Gogolak (1962). "The significance of the rabbit's septum as a relay station between the midbrain and the hippocampus I. The control of hippocampus arousal activity by the septum cells". In: *Electroencephalography and clinical neurophysiology* 14.2, pp. 202–211.

Pignatelli, Michele, Anna Beyeler, and Xavier Leinekugel (2012). "Neural circuits underlying the generation of theta oscillations". In: *Journal of Physiology-Paris* 106.3-4, pp. 81–92.

Santos-Pata, Diogo et al. (2021a). "Entorhinal mismatch: A model of self-supervised learning in the hippocampus". In: *Iscience* 24.4, p. 102364.

— (2021b). "Epistemic autonomy: self-supervised learning in the mammalian hippocampus". In: *Trends in Cognitive Sciences* 25.7, pp. 582–595.

Sławińska, Urszula and Stefan Kasicki (1998). "The frequency of rat's hippocampal theta rhythm is related to the speed of locomotion". In: *Brain research* 796.1-2, pp. 327–331.

Smear, Matthew et al. (2011). "Perception of sniff phase in mouse olfaction". In: *Nature* 479.7373, pp. 397–400.

Soltesz, Ivan and Attila Losonczy (2018). "CA1 pyramidal cell diversity enabling parallel information processing in the hippocampus". In: *Nature neuroscience* 21.4, pp. 484–493.

Stimberg, Marcel, Romain Brette, and Dan FM Goodman (2019). "Brian 2, an intuitive and efficient neural simulator". In: *Elife* 8, e47314.

Tsanov, Marian (2017). "Speed and oscillations: medial septum integration of attention and navigation". In: *Frontiers in systems neuroscience* 11, p. 67.

VanRullen, Rufin (2016). "Perceptual cycles". In: *Trends in cognitive sciences* 20.10, pp. 723–735.

VanRullen, Rufin, Rudy Guyonneau, and Simon J Thorpe (2005). "Spike times make sense". In: *Trends in neurosciences* 28.1, pp. 1–4.

Witter, Menno P et al. (2000). "Anatomical organization of the parahippocampal-hippocampal network". In: *Annals of the New York Academy of Sciences* 911.1, pp. 1–24.

Young, Calvin K, Ming Ruan, and Neil McNaughton (2020). "Speed modulation of hippocampal theta frequency and power predicts water maze learning". In: *BioRxiv*.

Annexes

A Derivation of the $I_s - \phi$ curve

The general solution for an equation of the type:

$$\tau_m \frac{dV}{dt} = -V + R_m I(t) \tag{29}$$

is:

$$V(t) = V_0 e^{-(t-t_0)/\tau_m} + \frac{R_m}{\tau_m} \int_{t_0}^{t} e^{-(t-t')/\tau_m} I(t') dt' \tag{30}$$

In Equation (7), the current has two components ($I(t') = I_s + I_{osc} \cos(\omega t' + \phi)$). We will therefore compute two different integrals to obtain Equation 30. The first is:

$$\frac{R_m}{\tau_m} \int_{t_0}^{t} e^{-(t-t')/\tau_m} I_s dt' = R_m I_s \Big(1 - e^{-(t-t_0)/\tau_m}\Big) \tag{31}$$

To obtain a solution with a single sinusoidal component, we will use that $\mathrm{Re}[\int f(x)dx] = \int \mathrm{Re}[f(x)dx]$ to compute the second integral:

$$\frac{R_m}{\tau_m} \int_{t_0}^{t} e^{-(t-t')/\tau_m} I_{osc} \cos(\omega t' + \phi) dt' = \frac{R_m}{\tau_m} \int_{t_0}^{t} e^{-(t-t')/\tau_m} I_{osc} \mathrm{Re}[e^{i(\omega t' + \phi)}] dt'$$

$$= \mathrm{Re}\Big[\frac{R_m e^{i\phi}}{\tau_m} \int_{t_0}^{t} e^{-(t-t')/\tau_m} I_{osc} e^{i\omega t')} dt'\Big] \tag{32}$$

$$\frac{1}{\tau_m} \int_{t_0}^{t} e^{-(t-t')/\tau_m} e^{i\omega t'} dt' = \frac{e^{i\omega t} - e^{i\omega t_0} e^{-(t-t_0)/\tau_m}}{1 + i\omega\tau_m} \tag{33}$$

We can now factor out and express in polar coordinates the following term:

$$\frac{e^{i\phi}}{1 + i\omega\tau_m} = e^{i\phi} \frac{1 - i\omega\tau_m}{1 + \omega^2\tau_m^2} = A e^{i\varphi} \Longrightarrow A = \frac{1}{\sqrt{1 + (\tau_m\omega)^2}} \quad , \quad \varphi = -\arctan(\omega\tau_m) + \phi \tag{34}$$

and then get the real part of the whole expression:

$$\mathrm{Re}\Big[\frac{R_m e^{i\phi}}{\tau_m} \int_{t_0}^{t} e^{-(t-t')/\tau_m} I_{osc} e^{i\omega t'} dt'\Big] = \mathrm{Re}\Big[R_m I_{osc} A e^{i\varphi} \Big(e^{iwt} - e^{iwt_0} e^{-(t-t_0)/\tau_m}\Big)\Big] \tag{35}$$

$$= R_m I_{osc} A \Big(\cos(\omega t + \varphi) - e^{-(t-t_0)/\tau_m} \cos(\omega t_0 + \varphi)\Big) \tag{36}$$

Substituting 31 and 36 in Equation 30, we obtain the membrane potential at any given time t:

$$V(t) = V_0 e^{-(t-t_0)/\tau_m} + R_m I_s \Big(1 - e^{-(t-t_0)/\tau_m}\Big) + R_m I_{osc} A \Big(\cos(\omega t + \varphi) - e^{-(t-t_0)/\tau_m} \cos(\omega t_0 + \varphi)\Big) \tag{37}$$

$$\varphi = -\arctan(\omega\tau_m) + \phi \tag{38}$$

$$A = \frac{1}{\sqrt{1 + (\tau_m\omega)^2}} \tag{39}$$

B Analysis of phase distributions

B.1 Free membrane potential

The stochastic dynamics of the membrane potential are well-known in the absence of a threshold (i.e., the *free membrane potential distribution*), which allows voltages to take any real value. In terms of dynamic equations, this is equivalent to ignoring the changes in V induced by Equation (8). The first and second moments of this distribution come from the integration of the deterministic and stochastic terms, respectively, in Equation (16):

$$\mu_V(t) \equiv \mathrm{E}[V(t)] = V_0 e^{-\Delta} + R_m I_s \Big(1 - e^{-\Delta}\Big) + R_m I_{osc} A \Big(\cos(\omega t + \varphi) - e^{-\Delta}\cos(\omega t_0 + \varphi)\Big) \quad (40)$$

$$\sigma_V^2(t) \equiv \mathrm{Var}[V(t)] = \eta V_{th} \frac{1 - e^{-2\Delta}}{2} \quad (41)$$

The probability density function of free voltage at time t is then given by:

$$p_{V_f}(V, t | V_0, t_0) = \frac{1}{\sqrt{2\pi\sigma_V^2(t)}} \exp\left(\frac{[V - \mu_V(t)]^2}{2\sigma_V^2(t)}\right) \quad (42)$$

While this distribution is transferred in a nonlinear manner to the spike time, which has in fact no known closed-form solution (due to the existence of a threshold), Equations (40)-(42) give a qualitative idea of the relationship of noise amplitude to σ_W and $f = 1/T$.

Effective current, transfer function, and local expansion of noise

A potential that evolves according to noisy dynamics will end up following a particular trajectory and producing a spike at a particular phase. Here we name *effective current* (I_{eff}) a tonic input I_s that, in the absence of noise, would have resulted in the same firing phase. The existence of such a value (or a reasonable approximation) allows us to study the propagation of noise with deterministic dynamics. Let's assume that such an effective current exists and, over trials, it follows a Gaussian distribution:

$$I_{eff} \sim \mathcal{N}(\mu_I, \sigma_I) \quad (43)$$

Then, the distribution of the membrane potential at time t that comes from sampling from I_{eff} and letting the voltages evolve according to deterministic dynamics is:

$$V(t; I_{eff}) \sim V_0 e^{-(t-t_0)/\tau_m} + R_m I_{eff}\Big(1 - e^{-(t-t_0)/\tau_m}\Big) + R_m I_{osc} A \Big(\cos(\omega t + \varphi) - e^{-(t-t_0)/\tau_m}\cos(\omega t_0 + \varphi)\Big) \quad (44)$$

Given that this distribution comes from a linear transformation of I_{eff}, $V(t)$ will have the following moments:

$$\mu_V = V(t; \mu_I) \quad (45)$$

$$\sigma_V = R_m \Big(1 - e^{-(t-t_0)/\tau_m}\Big)\sigma_I \quad (46)$$

The fact that we have obtained an expression very similar to Equation (37) with a single random variable suggests again the possibility of imposing phase locking ($t - t_0 = T$) to then isolate the phase ϕ, as done for Equation (15). However, there is the issue that precisely because now the effective current comes from a noisy integration of the trajectory, it will in general not hold

$t - t_0 = T$ (i.e., the neuron will fire slightly earlier or later). However, these deviations tend to cancel out and a good approximation of the distributions that still be obtained by assuming phase locking. Repeating the same manipulations than the ones to derive $\phi(I_s)$, but now to obtain a deterministic mapping over the distribution I_{eff}, we get:

$$\phi^{(s)} \sim \arccos\left(\frac{V_{th}}{RI_{osc}A\Big(1 - e^{-T/\tau_m}\Big)} - \frac{I_{eff}}{AI_{osc}}\right) - \varphi \tag{47}$$

This expression provides a *transfer function* that maps a value sampled from I_{eff} to a specific spike phase. If the value of σ_I is small enough, one can linearize around μ_I and obtain the corresponding distribution in the phase space:

$$\phi \sim \phi(I_s) + \phi'(I_s)\Big(I_{eff} - I_s\Big) \Longrightarrow \phi^{(s)} \sim \mathcal{N}\Big(\phi(\mu_I), |\phi'(\mu_I)|\sigma_I\Big) \tag{48}$$

The assumption that the linear expression is valid, and that I_{eff} can be reasonably described by a Gaussian distribution $\mathcal{N}\Big(\mu_I, \sigma_I\Big)$, comes from the fact that the obtained distributions in ϕ are themselves reasonably Gaussian, and only the linear mappings of Gaussian variables can result in Gaussian distributions.

We now present some results that aim to evaluate whether:

- An approximation for $I_{eff} \sim \mathcal{N}\Big(\mu_I, \sigma_I\Big)$ can be obtained from simulations.
- σ_I^2 is a monotonic function of the variance of the free voltage distribution estimated at the period of the oscillation $\sigma_V^2(T)$ (Equation (41)).

To test these hypotheses, we estimate I_{eff} from the ϕ distributions obtained in simulations by taking the inverse of Equation (48):

$$I_{eff} \sim I_s + \frac{\phi - \phi(I_s)}{\phi'(I_s)} \tag{49}$$

We observe that the degree of normality strongly depends on the region within the (f, σ_W) parameter space (Figure 7A). For instance, at a frequency of 5Hz, the Gaussian density function covers almost perfectly the obtained distributions, whereas at 30Hz that is not the case anymore. Another important observation is that the average of the distributions μ_I is very close to I_s, and indeed it behaves very similarly with respect to f (Figure 7B).

We then examine the relationship of the obtained values of σ_I to the oscillatory frequency and the amplitude of the white noise σ_W. As expected, we observe that σ_I decreases with frequency (since there is less time for noise integration), whereas it increases with σ_W (Figures 8A and B). The decrease of σ_I with frequency can be mainly observed at $f \geq 10$Hz (Figure 8A). In the $[0, 10]$ Hz interval, where we would expect a flat curve (as the exponential term in Equation (41) becomes almost negligible), there is instead a decrease in variance as $f \to 0$. This is due to the fact that very low frequencies allows the noise to generate a number of additional spikes per cycle (Figure 8C), which can in turn skip cycles and affect the distributions by reducing their variance due to the hard bound imposed by the phase space (detailed discussion of these effects can be found in section 2.1.2 in Results). Overall, and together with the observation that σ_I monotonically increases with σ_W (Figure 8B), the above results indeed confirm that the

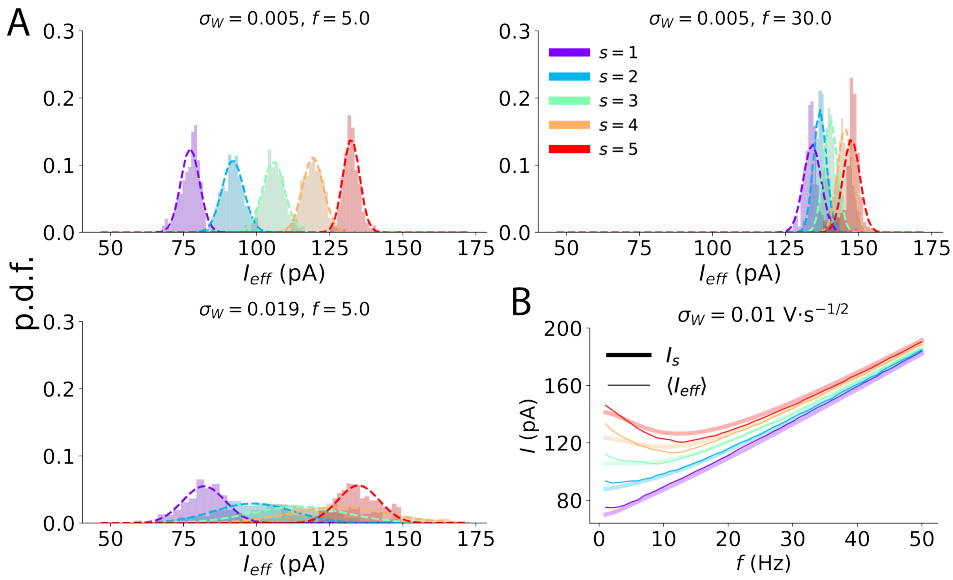

Figure 7: Effective current distributions and their relation to the tonic input A. Distributions of I_{eff} obtained in simulations as defined by Equation (49) for different input levels (see colors in the top-right panel). The dashed lines denote the Gaussian density functions defined by the means and variances obtained in simulation. **B.** Average of the effective current distribution (wide lines) and actual I_s values (thin lines), for different input levels, as a function of frequency.

standard deviation of the distributions obtained in I_{eff} (averaged over s) inherits the stochastic behavior of the noisy free membrane potential.

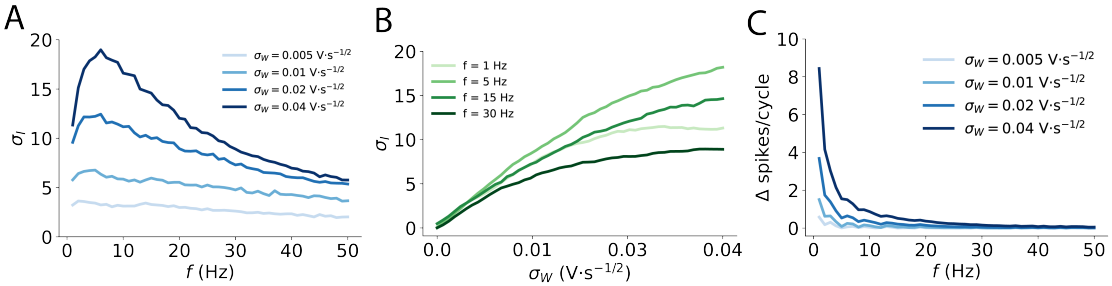

Figure 8: Variance of the effective current depends on the frequency and noise levels. A. σ_I as a function of frequency. **B.** σ_I as a function of noise. **C.** Expected number of additional spikes (averaged across all stimulus levels) observed for different noise levels, and taking $\sigma_W = 0$ as a baseline.